Valorization of marble powder wastes using rice husk ash to yield enhanced-performance inorganic polymer cements: Phase evolution, microstructure, and micromechanics analyses

Elie Kamseu [a,b,*], Ange-Therese Akono [c], Roberto Rosa [d], Alberto Mariani [e], Cristina Leonelli [b]

[a] *Department of Research, Local Materials Promotion Authority, P. O. Box 2396, Yaounde, Cameroon*
[b] *Dipartimento di Ingegneria "Enzo Ferrari", Università degli Studi di Modena e Reggio Emilia, Via P. Vivarelli 10, 41125, Modena, Italy*
[c] *Department of Civil and Environmental Engineering, Northwestern University, 2145, N Sheridan Rd., Evanston, Il, USA*
[d] *Dipartimento di Scienze e Metodi dell'Ingegneria, Università degli Studi di Modena e Reggio Emilia, Viale Amendola 2, 42122, Reggio Emilia, Italy*
[e] *Dipartimento di Chimica e Farmacia, Università di Sassari, and Local INSTM Unit, Via Vienna 2, 07100, Sassari, Italy*

ARTICLE INFO

ABSTRACT

The challenge for sustainable development is now constraining scientists, and policymakers to consider alternative materials and processes requiring low energy consumption and low emissions while prioritizing local materials and industrial waste recycling. This study investigates ways to valorize marble waste powders to design a new class of inorganic polymer cement. These powders are among the most important solid wastes globally, and in the Italian island of Sardinia they create a disposal problem. When these powders, which are rich in calcium silicate hydrate (C–S–H) phases, are incorporated into the geopolymer synthesis, this gives rise to a mix between C–S–H and alkali metal aluminosilicate hydrate (M-A-S-H) systems that are the focus of this study. In detail, C–S–H systems are prepared with various Ca/Si ratios, including CS, C_2S, and C_3S. The microstructure and mechanical properties are investigated using X-ray diffraction, Fourier transform infrared spectroscopy, and scanning electron microscopy, along with density methods (mercury intrusion porosimetry), macroscopy mechanical testing methods (flexural strength tests) and nanoscale mechanical testing methods (indentation testing and scratch testing). The resulting inorganic polymer cements exhibit both an amorphous and a crystalline phase containing sodium-calcium-aluminum-silicate hydrate N–C-A-S-H. The fraction of the crystalline phase increases when the silica content decreases, from CS to C_3S, and when the C–S–H fraction increases. In turn, the crystalline phase dictates the pore structure and mechanical properties. Specifically, a homogeneous and compact microstructure with low porosity is observed. The flexural strength ranges from 5.8 to 8.7 MPa, the elastic modulus ranges from 10 to 17 GPa, and the fracture toughness ranges from 0.23 to 0.48 MPa $m^{1/2}$. In general, the lower the silica percentage of the calcium-silicate hydrates and the higher the fraction of calcium silicate hydrate are, the higher the flexural strength, elastic modulus, and fracture toughness. The underlying mechanism for the observed stiffening, strengthening, and toughening is the insertion of aluminum in the C–S–H defect sites to yield C-A-S-H, along with the formation of sodium silicate gel from excess colloidal silica, which contributes to the reduction in gel pores and matrix densification. The values of porosity, density, and mechanical properties suggest that inorganic polymer cements derived from marble wastes are promising candidates for innovative low-temperature and low-density binders with low carbon footprint satisfying both the requirements of sustainability and the local material concept.

1. Introduction

The challenge for sustainable development is now constraining scientists and policymakers to propose alternative materials and processes requiring low energy consumption and low emissions, such as alkali-activated cements (Shi et al., 2011). One of the key elements that accounts for the sustainability of a binder or structural composite but is rarely considered is the local materials concept. For instance, the local availability and selection of solid raw precursors for the production of alkali-activated binders significantly contributes to their low carbon

---

footprint (Provis, 2018) and strongly affect the property of the resulting binders (Kamseu et al., 2021a). Within the concept of cleaner production, to protect the environment, it is strongly recommended to use locally available raw materials and minimize wastes, such as waste glasses (Liu et al., 2019) or fly ash (Fernandez-Jimenez et al., 2006) and emissions while prioritizing renewable materials and energy. In the line of sustainability, geopolymers and alkali-activated cements are subjected to excessive criticism and doubts given the alkali-activating solution (Li et al., 2018). Habert et al. (2011) have suggested that the use of a sodium silicate-activating solution can increase the environmental impact of geopolymer concretes. Kamseu et al. (2021a,b), while describing the sustainability conditions of geopolymers, indicated their dependence on raw solid precursors. As a result, regions where basic raw materials and wastes for calcium silicate hydrate (C–S–H) production abound should focus on appropriate processes involving these basic raw materials and wastes for geopolymer production for reducing energy and CO_2 emissions; otherwise, the final binder will neither be cleaner nor sustainable.

The primary aim of this study is to investigate ways to valorize marble waste powders to design a new class of inorganic polymer cement. These powders represent one of the most important solid wastes globally in general, and in the Italian island of Sardinia in particular, with marble waste representing 70% of the final product obtained from the marble industry (Mehta et al., 2020). Many Ca-rich cementitious materials have been described in the literature using industrial wastes, usually fly ash and slag; the most common issues are particle dissolution and reactivity rate, as well as the presence of unreacted particles. Few studies have investigated the recycling of marble powder waste for geopolymer technology. Most studies of marble valorization have focused on its use as a cement admixture or concrete aggregate. For instance, Sharma and Kumar (2015) reported a decrease in both the compressive and cement tensile strength of cement when marble powder is used as a sand substitute in Portland cement with a sand replacement ratio greater than 10% (Sharma and Kumar, 2015). Alyousef et al. (2019) investigated the use of marble waste to modify self-compacting concrete. They found that, although marble waste incorporation improves the air content and carbonation resistance, the compressive strength is reduced. The decrease in the compressive strength was attributed to the reduction in the fraction of reactive silica in the mix (Benjeddou et al., 2020). Similarly, Kechagia et al. (2021) found that marble waste led to a decrease in the compressive strength when used as cement admixture, due to the formation of ettringite. An attempt to mix marble powder waste with soda lime recycled glass for improved reactivity did not improve the mechanical performance. Few studies have investigated the use of marble powder waste for the synthesis of alkali-activated materials. Komnitsas et al. (2021) investigated the use of marble powder waste to synthesize metakaolin-based alkali-activatd materials. They observed the formation of a hybrid N–C–A–S–H phase. They reported a decrease in compressive strength and an increase in porosity. They concluded that marble powder waste exhibit a low reactivity due to their low Si and Al content and they recommended mixing marble powder waster with other wastes with a high Si and Al content. In brief, the major issue in valorizing marble powder waste is their low reactivity, and it is recommended to combine marble powder waste with other waste type for improved reactivity. Building on Komnitas et al.'s study, we investigate the use of marble powder waste together with rice husk ash to yield inorganic polymer cements with higher reactivity, lower porosity, and improved mechanical properties.

On one hand, wastes for C–S–H production are particularly appealing, given the possibility of being produced at low temperatures (<100 °C) to yield eco-friendly C–S–H-based binders, for instance using rice hull ash (RHA) recycled from biomass (Rodrigues, 2003) or low-lime calcium silicates (Ahsraf and Olek, 2016). These binders are promising candidates that have been classified as suitable binders, with applications in repairing mortar (Chindaprasirt et al., 2022) and geothermal well cement (Kuzielová et al., 2017), which require fast

setting, non-shrinkage, and acid-resistant properties. In fact, for cement applications in oil wells and geothermal wells, where the temperature can exceed 120 °C, the calcium silicate hydrate itself is too weak and permeable to seal the well (Carter and Smith, 1958). In contrast, scientific data available in the literature indicates the improvement in C–S–H matrices through the addition of reactive alumina (Fernandez-Jimenez et al., 2006). Here, it is postulated that the incorporation of Al^{3+} will favor the development of the calcium-aluminate-silicate-hydrate (C-A-S-H) phases with a significant improvement in the mechanical properties and resistance to sulfates and acids (Dharmawardhanaa et al., 2018). The incorporation of Al_2O_3 facilitates the design of matrices with fibrillar morphology without significantly affecting the final density, which leads to an increase in the amount of interlayer water and a decrease in the fraction of gel porosity (Avet et al., 2019). Consequently, the C-A-S-H system resulting from the incorporation of Al_2O_3 in C–S–H phase facilitates the thermal stability of the final binders, hindering the formation of micro-porosity and degradation of the mechanical properties at relatively high temperatures (200 °C).

A microstructural analysis yields insights into the improvement of C–S–H matrices through Al^{3+} incorporation. A microstructural interpretation of C–S–H phase presents silica chains that represent the Dreirketten arrangement: two tetrahedral pairing the calcium oxide layers and a third bridging to the next pair of silicates (Richardson, 2008). However, the main defects generally ascribed to C–S–H structures are missing bridging silicate tetrahedra and the substitution of two protons terminated by calcium ions into the interlayer. When C–S–H is transformed into C-A-S-H phase, Al^{3+} occupies bridging sites that link the dimers of the silicate tetrahedral (Dharmawardhanaa et al., 2018), which might lead to an increase in the average chain length. The C-A-S-H phases formed in concrete are X-ray amorphous (Provis et al., 2005) with largely varying compositions, which exhibit high structural heterogeneity, as C–S–H is finely mixed with other phases, including impurities and water content (Myers et al., 2013).

In contrast, the alkali metal aluminosilicate hydrate-type gel—also known as M-A-S-H, where M represents the alkali metal in the activator—results from the dissolution of metakaolin into an alkali-activating solution. The alkali metal promotes the development of a structurally disordered and highly cross-linked M-A-S-H gel (Duxson et al., 2005a,b). The high pH provided by the activator facilitates the leaching of Al and Si from the precursor particles, which then precipitate and polymerize through condensation reactions to form a geopolymer gel. Al and Si in the M-A-S-H gel network are present in tetrahedral coordination, with silica in a Q^4(mAl) ($0 \leq m \leq 4$)-type environment (Matsuyana and Young, 2008). The silica-to-alumina or silicon-to-aluminium ratio plays a fundamental role in the hydrolysis, dissolution, and polymerization/polycondensation processes (Duxson et al., 2005a,b), as well as in the intrinsic mechanical properties, where numerous Q^4(3 A l) and Q^4(2 A l) sites (resulting from a relative increase in Si content in the system) yield higher mechanical strength. Finally, the composition and quantity of the M-A-S-H gel formed during geopolymerization are dependent on the degree of reactivity of the solid precursor; in turn, the reactivity of the solid precursor is related to the reactive oxide content, chemical composition, and particle size and morphology.

When the wastes for C–S–H production are incorporated into the geopolymer synthesis, a mix between C–S–H and alkali metal aluminosilicate hydrate (M-A-S-H) systems is obtained.. In this study, C–S–H systems are prepared with various Ca/Si ratios, including CS, C_2S, and C_3S, in a way to increase the probability of covering the C–S–H(I) and C–S–H(II) gel described in the literature (Allen et al., 2007). The different C–S–H gels developed are mixed with a typical metakaolin-based geopolymer gel (M-A-S-H).

In this study, a vast array of experimental methods is utilized to explore the characteristics of the C–S–H/N-A-S-H cement (Na was chosen as alkali metal in this investigation), —including flexural strength tests; depth-based nanomechanical characterization methods, such as

scratch tests and indentation tests; mercury intrusion porosimetry tests; environmental scanning electron microscopy; X-ray diffraction tests; and Fourier transform infrared spectroscopy tests.

2. Materials and methods

2.1. Materials

Calcium silicates with three different molar ratios of 1:1 (CaO:SiO$_2$– CS), 2:1 (2CaO:SiO$_2$–C$_2$S), and 3:1 (3CaO:SiO$_2$–C$_3$S) were used as partial replacements of metakaolin-based geopolymer cement. C–S–H/N-A-S-H phases were obtained from the incorporation of 40–70 wt% (Table 1) of C–S–H paste into N-A-S-H paste by mixing the two pastes previously prepared a few minutes before at room temperature. The calcium silicate powders used were prepared at a low temperature (~100 °C) using calcined recycled powders of marble and RHA, as detailed in (Kamseu et al., 2021b). Water was added to the different calcium silicate powders in 0.35–0.4 liquid/solid weight ratios to yield C–S–H pastes. The C–S–H pastes were prepared from a highly reactive grade of cementitious materials. The N-A-S-H paste was synthesized using metakaolin that was prepared from high-grade kaolin by calcination at 700 °C for 4 h (Kamseu et al., 2013). A mix of sodium hydroxide (8 M) and sodium silicate (SiO$_2$/Na$_2$O molar ratio = 3.00) in 1:1 vol ratio was used as the alkaline solution for preparing N-A-H gel with a solid-to-liquid weight ratio of 1.6. The sodium hydroxide solution was prepared using a parent solution with 50 wt% of Na$_2$O. Both the sodium silicate solution and parent sodium hydroxide solution were from Ingessil srl. Verona, Italy. The mix proportions for the C–S–H and N-A-S-H pastes are listed in Table 1. The C–S–H and N-A-S-H pastes were ball-milled together for 5 min at 1200 rpm, and the resulting paste was poured into Teflon molds. All specimens in the Teflon molds were sealed into plastic bags for 24 h before demolding, and the curing continued in the sealed plastic bags for a minimum of 72 h. The final inorganic polymers were characterized at least 28 d after demolding.

2.2. Methods

2.2.1. X-ray diffraction

The phases present in the raw precursors (calcium silicates: CS, C$_2$S, and C$_3$S) are detailed in (Kamseu et al., 2021b). Phase characterization for the different grades of C-A-S-H-based binders was performed in fine-grounded powders using an X-ray powder diffractometer: XRD (PW3710; Philips) Cu, Kα with Ni-filtered radiation having a wavelength of 1.54184 Å. This diffractometer used radiation generated at 40 mA and 40 kV. Specimens were scanned as random powder with a 2θ range of 5°–70° and integrated at the range of 2 s per step.

2.2.2. Fourier transform infrared spectroscopy

Fourier transform infrared (FTIR) spectroscopy equipment (Avatar 330 Thermo Nicolet) was used to collect the spectra of the inorganic polymer powders. A minimum of 32 scans between 4000 and 400 cm^{-1} were considered for CS, C$_2$S, and C$_3$S series with intervals of 1 cm^{-1}.

2.2.3. Grinding and polishing

The inorganic polymer binder specimens were polished for nanoscale mechanical testing through scratch testing and indentation testing. Each sample was embedded in low-viscosity epoxy resin and then cut into 3-

mm-thick slices using a low-speed diamond saw. The thin slices were then glued onto aluminum disks using cyanoacrylate adhesive for further grinding and polishing. Grinding was conducted using a semi-automated grinder polisher along with silicon carbide pads of consecutive grit sizes of #240, #400, and #600. Polishing was performed manually using silicon carbide pads of particle sizes of 3, 1, and 0.25 μm. Between each step, the specimens were cleaned using an ultrasonic bath with n-decane to prevent cross-contamination. After grinding and polishing, the specimens were stored in a desiccator under vacuum until further testing.

2.2.4. Mercury intrusion porosimetry tests

Specimens of approximately 2 cm^3 dimensions were prepared for the mercury intrusion porosimetry (MIP) analysis using a Micromeritics autopore IV 9500. The specimens were placed into a penetrometer, and their porosity and pore size distribution were evaluated using an equilibrium of 10 s mode and pressure limits of 345 kPa and 228 MPa to measure pores with diameters ranging from 0.006 to 350 μm.

2.2.5. Scanning electron microscopy

The microstructure of unpolished inorganic polymer cement was analyzed using an environmental scanning electron microscope (ESEM). The equipment was a Quanta 200, FEI Co., operating at a current of 30 mA and voltage of 25 kV. Fresh fractured pieces of inorganic polymer cement from the mechanical testing were collected and fixed into an aluminum tap with a 10-nm silver/gold coating before the observations. In addition, high-resolution backscattered environmental scanning electron microscopy (BESEM) was used to visualize the microstructures of polished inorganic polymer cements. BESEM was conducted using an FEI Quanta 650 ESEM in low-vacuum mode with a working distance of 7–10 mm, an accelerating voltage of 10–15 kV, and magnification levels of × 1000–20,000.

2.2.6. Flexural strength tests

The three-point flexural strength of the inorganic polymer binders was determined with an Instron 1195 machine having a displacement rate of 3 mm/min. Four specimens were tested for each inorganic polymer material, and the average flexural strength was determined. The dimensions of the tested specimens were 140 ± 0.1 mm for length l and 10 ± 0.05 mm for width b and thickness h. The flexural strength $σ$ was computed from the maximum load F at fracture, as follows:

$$\sigma = \frac{3Fl}{2bh^2} \tag{1}$$

2.2.7. Indentation testing

Indentation tests were performed to probe the elastoplastic characteristics and microphase distribution. All tests were conducted using an Anton Paar (Ashland, VA) microhardness tester equipped with a 2-nm-radius Berkovich indenter. During each test, the indenter was pressed against the material, and a trapezoidal vertical load was applied. The maximum vertical force was 2 mN, the loading/unloading rate was 4 mN/min, and the holding period was 10 s. For each indentation test, the indentation modulus M and indentation hardness H were computed using Oliver and Pharr's model (Oliver and Pharr, 1992):

$$M = \frac{\sqrt{\pi}}{2} \frac{S}{\sqrt{A(h)}}; \quad H = \frac{P_{max}}{A(h)} \tag{3}$$

Here, h is the penetration depth, A is the projected contact area, S is the unloading slope, and P$_{max}$ is the maximum vertical force. The projected contact area function A(h) was calibrated prior to testing using fused silica as the reference material.

The microphase distribution was computed using statistical nanoindentation. For this purpose, nanoindentation grids were used (16 × 16 indents for specimens C$_2$S40 and C$_3$S40 and 25 × 25 indents for the remaining specimens) with a 25 μm microindent spacing. Statistical

Table 1
Mix design of inorganic polymer cements.

Weight percentage (%) of calcium silicate addition			
40	50	60	70
CS40	CS50	CS60	CS70
C$_2$S40	C$_2$S50	C$_2$S60	C$_2$S70
C$_3$S40	C$_3$S50	C$_3$S60	C$_3$S70

deconvolution was then performed. The principle of statistical deconvolution is to write the distribution of the indentation hardness and indentation modulus as a weighted sum of individual Gaussian distributions (Ulm et al., 2007) and the method has been successfully used to resolve chemomechanical phases in cementitious materials (Sorelli et al., 2008). Here, statistical deconvolution was conducted using a custom-made algorithm written in the Python computer programming language.

2.2.8. Scratch testing

Scratch tests were employed to characterize the fracture response. The principle of scratch testing is to push a diamond sphero-conical probe across the specimen surface under a linearly increasing vertical force while recording the horizontal force and penetration depth. All scratch tests were conducted using an Anton Paar (Ashland, VA) microscopic scratch tester. Prior to the test, the reference surface was assessed using a surface profilometer with a contact load of 0.03 N. In all tests, a Rockwell C diamond probe was used, which comprises a cone of half-apex angle 60 °C, terminated by a sphere of radius R = 200 μm. The maximum vertical force was 5.5 N, the scratch length was 3 mm, and the scratch speed was 6 mm/min. For each specimen, N = 8 scratch tests were conducted. During each scratch test, the forces and penetration depth were assessed using high-resolution load sensors and displacement transducers at an acquisition rate of 45 kHz. The fracture toughness was computed from the forces and depth measurement under the application of a nonlinear fracture mechanics model that assumes a semi-circular crack beneath the indenter (Akono et al., 2011). The premise of the theoretical model is to compute the energy release during a scratch-induced fracture process from the perspective of an observer tied to the tip of a propagating crack (Akono and Ulm, 2012). The final equation relating the forces and penetration depth to the fracture toughness K_c can be expressed as follows (Akono et al., 2012):

$$F_T = K_c \sqrt{2pA_{LB}(d)} \qquad (2)$$

where F_T is the horizontal force, d is the penetration depth, and $2pA_{LB}$ is the scratch probe shape function, which is calibrated using a reference material, such as fused silica, prior to testing. For instance, for tests conducted in the spherical range, with a penetration depth of less than 27 μm, the calibration function can be expressed as follows: $\frac{2pA_{LB}}{R^3} = 54.51 \left(\frac{d}{R}\right)^2$ (Akono and Ulm, 2014).

3. Results

3.1. Phases identification

3.1.1. XRD results

The XRD patterns of inorganic polymer binders are presented in Fig. 1. When N-A-S-H and C–S–H are mixed, there is evidence of the dissolution of amorphous Al_2O_3 and SiO_2 with the formation of aluminate and silicate oligomers. In this chemical context, there exists a high potential for the substitution of Si by Al into C–S–H chains, including the replacement of Ca by Na. These phenomena seem more applicable when high calcium silicate is used, in particular when C_3S is considered. The increase in the interactions between N-A-S-H and C–S–H favors the formation of a more crystalline C-A-S-H, particularly with a high Ca content. Consequently, the XRD spectra show a mix of both amorphous and crystalline phases, with the amorphous-to-crystalline ratio being a function of the type and replacement fraction of calcium silicate.

In particular, the lower the amount of calcium, the more amorphous is the resulting inorganic polymer. For instance, a CS40 matrix appears with a high volume of amorphous-phase characteristics of the
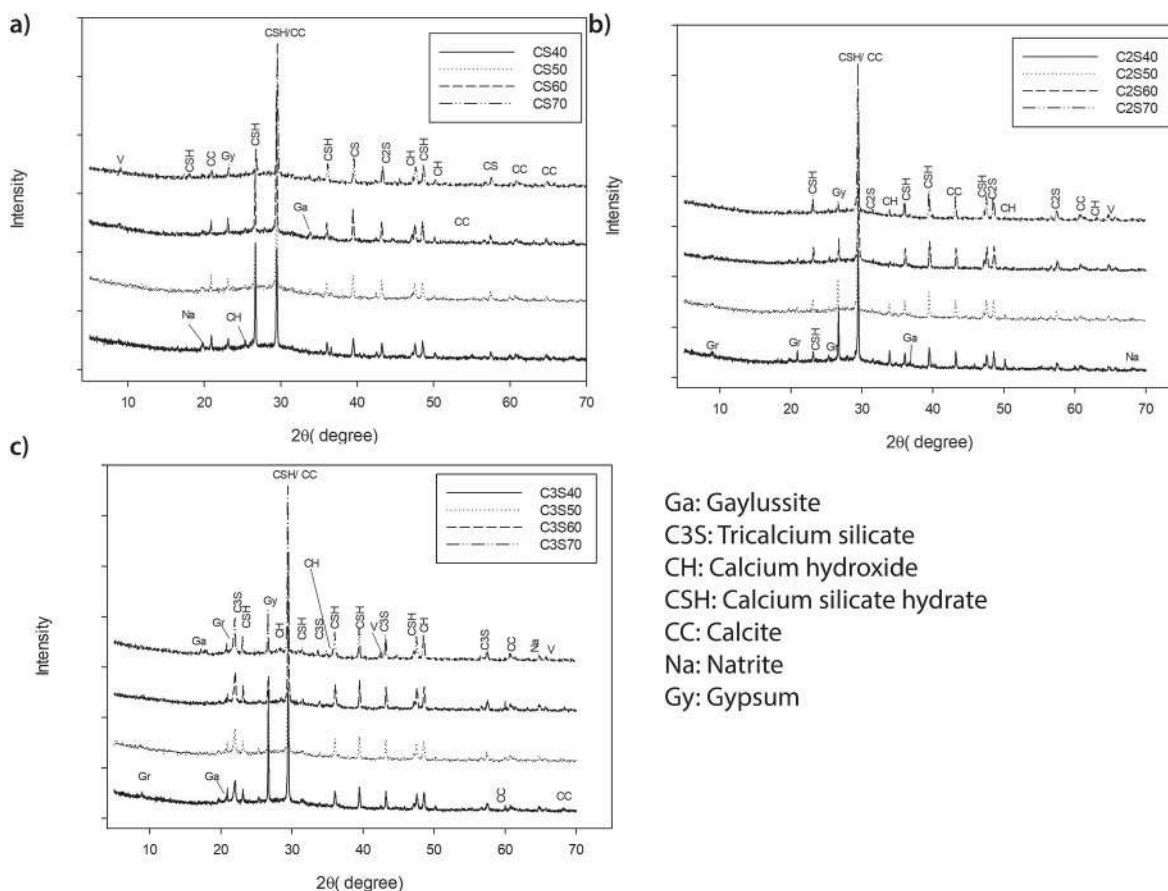

Ga: Gaylussite
C3S: Tricalcium silicate
CH: Calcium hydroxide
CSH: Calcium silicate hydrate
CC: Calcite
Na: Natrite
Gy: Gypsum

Fig. 1. XRD patterns of inorganic polymer cement: a) CS series, b) C_2S series, and c) C_3S series.

geopolymer. In turn, C_2S40 appears to exhibit slightly improved crystallinity with respect to CS40. Finally, C_3S40 shows XRD patterns with more peaks of crystalline phases with significant intensities conducing to a matrix with less amorphous content (Fig. 1c).

Moreover, the higher the C–S–H fraction, the more crystalline is the resulting inorganic polymer. In this case, the progressive replacement of N-A-S-H with C–S–H tends to enhance the volume of crystalline phases that should be C-(A)-S-H; consequently, the volume of the amorphous phase decreases for the series CS40, CS50, CS60, and CS70 (Fig. 1b). Another reason is the alkalinity of the matrix, which increases with the C–S–H fraction and significantly impacts the C–S–H-based phases with consequent potential of reduction in crystallinity. Finally, the XRD spectra show peaks of calcite into the matrices, which refers to the high level of reactivity of calcium silicate used as one of the solid precursors in this investigation.

3.1.2. FTIR results

The decrease in the silica content from CS to C_2S and C_3S leads to a decrease in the wavelength of the peak of the principal band and a reduction in the amount of Q^3 and Q^4 silica, which is characteristic of amorphous phases. This trend explains a progressive change in crystallinity from highly amorphous to more crystalline when the calcium silicate (CS) type is replaced with C_2S and C_3S types.

The principal band characteristic of Si–O–Ca and Si–Al–Na has a peak at 975 cm^{-1} when 40 wt% of metakaolin-based geopolymer is replaced by CS (Fig. 2a). In the inorganic polymer cement with the CS series, the principal band of aluminosilicate shifts from 975 cm^{-1} (40 wt % of CS addition) to 990 cm^{-1} when 50 wt% of CS is added. Further addition of CS does not modify the band position. However, the principal band broadens with evidence of an increase in the amount of Q^2 silica when the amount of CS reaches 70 wt%. Q^2 silica is also unreacted silica, which is observed in the CS series of inorganic polymer cement as residual silica obtained from CS. There is also an increase in Q^3 and Q^4 silica, particularly when the CS percentage reaches 70 wt%. The peak of the principal band is very broad, especially for the low-wavelengths, which indicates the development of many amorphous phases, including Si–Al–Ca and Si–Al–Na, as gels.

With the C_2S series, the principal band is observed at 984 cm^{-1} when 40 wt% of C_2S is added to metakaolin-based geopolymer cement. The increase of the calcium silicate hydrate to 50 wt% maintains the principal band, with a peak not far from 984 cm^{-1}. The peak of the principal band moves to 990 cm^{-1} only with the addition of 70 wt% of C_2S. Here, no broad band is developed, and only a slight increase in the peak intensity is observed (Fig. 2b). This confirms the absence of Q^3 and Q^4 silicate in this series, unlike the CS series.

With the C_3S series, the principal band is maintained at 974 cm^{-1} when 40 wt% of C_3S is added to the metakaolin-based geopolymer cement. An increase of up to 50 wt% in the calcium silicate content does not modify the position of the peak of the principal band (Fig. 2c), which shifts to 979 cm^{-1} when 60 or 70 wt% of C_3S is added.

The formation of residual carbonates is observed through the intensities of the peak FTIR bands centered at 1450 cm^{-1}; the intensities of these peaks are a function of the calcium silicate fraction used. Even though the cementitious phases remain the principal product of the interactions between N-A-S-H and C–S–H, the suitable reactivity of both components, particularly the mobility of Ca and Na ions, results in the formation of residual carbonates that are part of the matrices described in this study (Fig. 2).

The addition of N-A-S-H phases to cementitious phases of the CS series makes the band characteristics of water (3300–3400 cm^{-1}) shift to lower wavelengths with the bands becoming broad (Fig. 2a–c). This indicates changes in the water content and chemical environments of OH bonds with the progressive dominance of C-(A)-S-H in the replacement of N-A-S-H, where (A) indicates a probable presence of Al atoms in C–S–H structure. The other band characteristic of the OH bonds of water (1647 cm^{-1}) remains more stable.
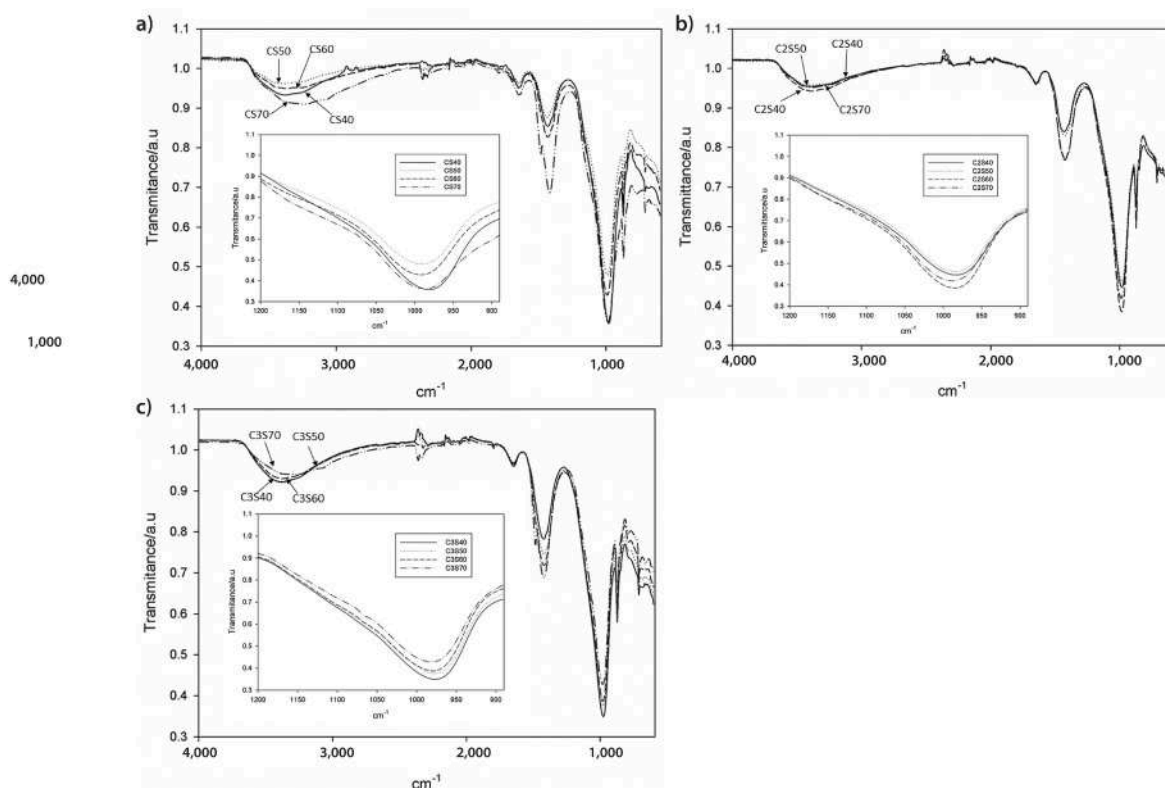

Fig. 2. FTIR spectra of inorganic polymer cement: a) CS series, b) C_2S series, and c) C_3S series.

3.2. Density, cumulative pore volume, and pore size distribution

3.2.1. Density results

The values of the densities obtained from the helium pycnometer and the measure of mass per volume are summarized in Fig. 3 and Table 2. Fig. 3 shows that the inorganic polymer cements produced have almost similar bulk density values (between 1.35 and 1.39 g/cm^3) when the C–S–H fraction is at 40 wt%. These values are not far from those of the density of the standard metakaolin-based geopolymer as compared to those available in the literature (Ribeiro et al., 2017).

When the C–S–H fraction exceeds 50 wt%, several behaviors are observed. The C$_3$S series remains stable with a density close to 1.40 g/cm^3. The C$_2$S series becomes lighter as the density decreases below 1.30 g/cm^3. In turn, for the CS series, the density first decreases and then increases to a high value of 1.70 g/cm^3 for 70 wt% CS.

3.2.2. Cumulative pore volume results

Fig. 4 presents the variation in the cumulative pore volume of the inorganic polymer cements as a function of the CS content and for the three series, CS, C$_2$S, and C$_3$S. The substitution of the metakaolin-based geopolymer paste with 40 wt% of C–S–H leads to cumulative pore volumes of 0.23, 0.29, and 0.28 mL/g, for the CS, C$_2$S, and C$_3$S series (Fig. 4). While the values for C$_2$S and C$_3$S series are similar to what is generally observed for the standard metakaolin geopolymer (Rovnaník, 2010), the cumulative pore volume decreases in the case of the CS series. When the mix is developed with 50 or 70 wt% of C$_2$S and C$_3$S, the cumulative pore volume remains almost constant at 0.29 mL/g.

3.2.3. Pore size distribution results

The dominance of CS in the mix results in pore size reduction in all formulations (Fig. 5), and the fraction of gel pores less than 20 nm in diameter significantly decreases when the C–S–H fraction increases. In fact, in the CS series, two principal bands are observed, with first peaks observed between 0.027 and 0.065 μm and the second band observed between 0.120 and 0.424 μm. At 70 wt% CS, both bands significantly decrease (Fig. 5c). Only certain small bands are observed in the respective regions of CS40 and C$_2$S50. The interstitial space has more volume in CS40 (0.23 mL/g) than that in CS70 (0.09 mL/g). The band

Table 2

Mechanical properties of individual microphases for inorganic polymer composites. M is the indentation modulus and H is the indentation hardness. MK GP = amorphous metakaolin geopolymer. N/C-A-S-H = sodium/calcium aluminosilicate hydrates.

Phase	Volume fraction (%)	**M**(GPa)	**H**(GPa)
C$_2$S40			
MK GP	73	5.33	0.11
MK GP	17	9.99	0.32
N–C–A–S–H	5	14.78	0.52
N–C–A–S–H	5	27.75	0.80
C$_2$S70			
MK GP	78	11.51	0.35
N–C–A–S–H	12	22.33	0.90
N–C–A–S–H	5	30.36	1.29
N–C–A–S–H	5	37.61	1.91
C$_3$S40			
MK GP	75	8.52	0.08
N–C–A–S–H	14	14.67	0.29
N–C–A–S–H	6	20.23	0.54
N–C–A–S–H	5	26.40	0.92
C$_3$S70			
MK GP	69	6.82	0.18
N–C–A–S–H	17	16.02	0.69
N–C–A–S–H	7	23.50	1.19
N–C–A–S–H	7	37.41	1.91

intensities of pores between 0.02 and 0.065 μm diameters and those between 0.12 and 0.424 μm in CS40 seem to significantly decrease when 70 wt% of calcium silicate CS is used (Fig. 6a). Certain small bands of capillary pores appear in the regions with a pore size of approximately 9.4 μm. However, the reduction in pore size is evident in Fig. 4c, where the cumulative pore volume is very low at 0.097 mL/g as compared to those of the other series. The cumulative pore volume here is remarkably low with a significant reduction in gel pores.

3.3. Microstructure

The BESEM results reveal a homogeneous microstructure with high
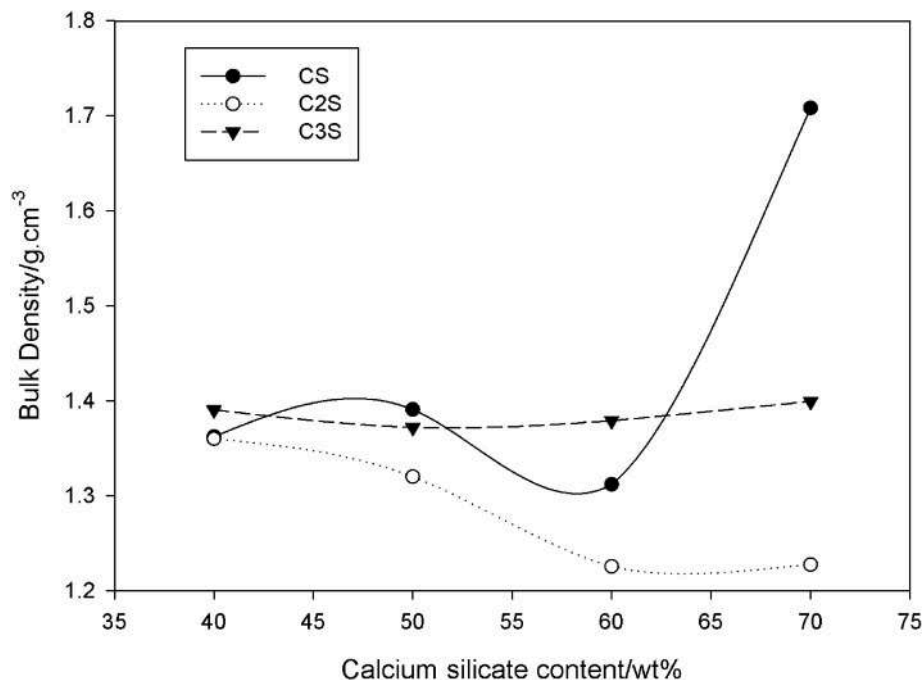
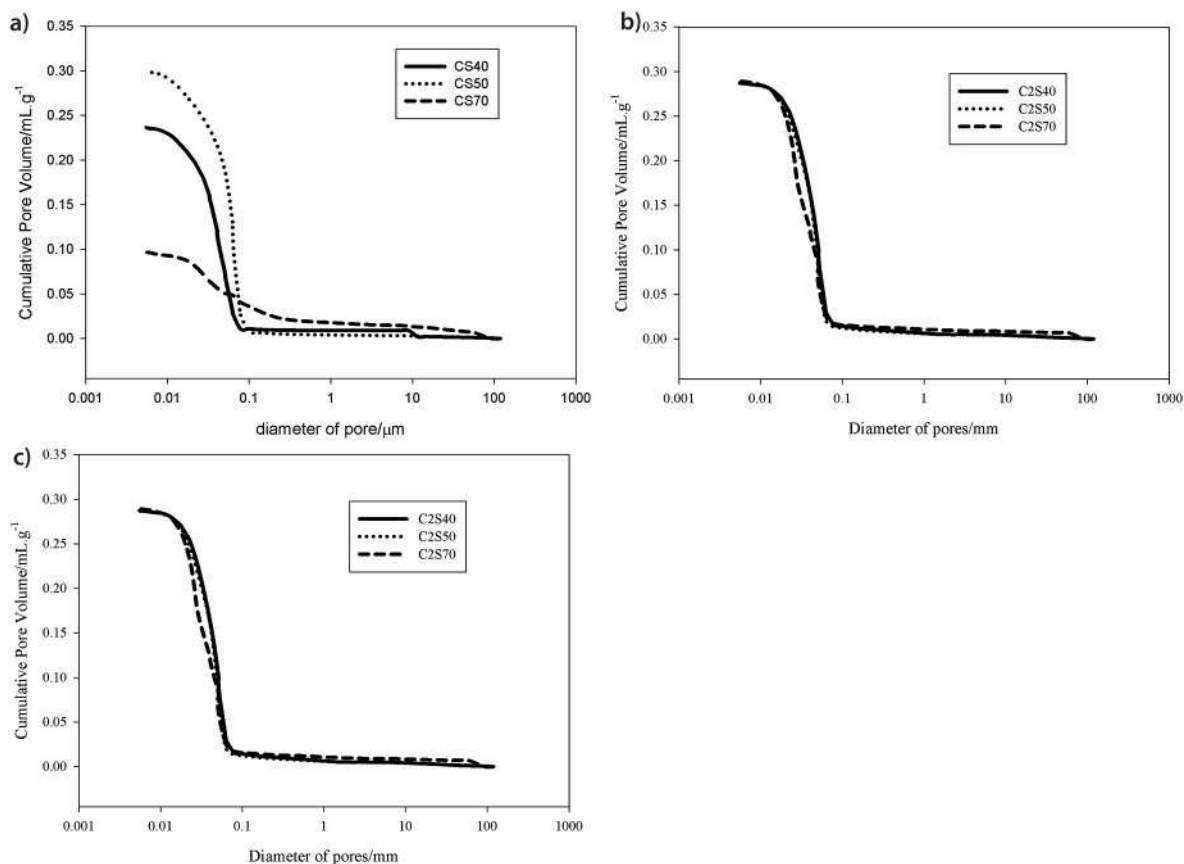**Fig. 3.** Bulk density of inorganic polymer cement as a function of calcium silicate content.

Fig. 4. Cumulative pore volume of inorganic polymer cement: a) CS series, b) C_2S series, and c) C_3S series.

compactness for the inorganic polymer cement paste made from CS (Fig. 6). At low magnification, the material is almost featureless, with suitable densification and compactness. At high magnification (Fig. 6b, d, and f), the gel comprises globular units (<100 nm in diameter) bonded to one another, developing extended long chains of aggregations (CS40) with amorphous silica acting as cement. The compactness of the inorganic polymer cements increases with the C–S–H fraction.

The inorganic polymer cement designed in this study is a nanoporous matrix. Fig. 7 displays high-resolution BESEM images of N–C-A-S-H phases for specimens CS70, C_2S70, and C_3S70 at a magnification of × 20,000. The radius, packing density, and cohesion of the grains vary with the inorganic polymer due to the difference in the concentration of the amorphous content, as already indicated through the XRD analysis. The average grain radius is 150 nm for CS70, 550 nm for C_2S70, and 250 nm for C_3S70. The grain radius agrees with the MIP observations of a secondary band of air voids in the 120–424 nm range (Figs. 4 and 5). Similarly, the grain radius for amorphous metakaolin-geopolymer (*i.e.*, 30–40 nm) (Kriven et al., 2006) agrees with the MIP observations of a primary band of air void in the 27–65 nm range. A multiphase structure is observed with two phases, metakaolin-geopolymer and N–C-A-S-H, characterized by two different length scales (*i.e.*, ~30 nm and 150–250 nm).

3.4. Mechanical properties

3.4.1. Flexural strength results

Fig. 8 displays the flexural strength of inorganic polymer cement as a function of the calcium silicate hydrates fraction. Overall, the flexural strength increases when the silica content is low, from CS, C_2S, to C_3S. The flexural strength also increases with the C–S–H fraction.

The specimens with 40 wt% of calcium silicate—CS or C_2S—show similar values of flexural strength (*i.e.*, 5.8 MPa); the specimens of the C_3S series exhibit slightly lower values of flexural strength (*i.e.*, 5.3 MPa). When the C–S–H fraction increases to 50 wt%, the flexural strength increases to 5.8, 6.0, and 6.4 MPa for C_3S, C_2S, and CS. Further addition of C–S–H (60 wt%) yields to a stable flexural strength of C_3S- and C_2S-based specimens (Fig. 8). The flexural strength of CS-based specimens increases significantly and reaches 7.3 MPa. Finally, when the C–S–H fraction reaches 70 wt%, the flexural strength of the C_2S- and C_3S-based formulations remains at 5.8 MPa; the values for the CS series increase up to 8.7 MPa.

3.4.2. Indentation modulus and indentation hardness

Fig. 9 displays the values of the indentation modulus and indentation hardness for the respective inorganic polymer cements. C_2S40, and C_3S40 have indentation modulus values of 7.27 GPa and 11.06 GPa, values which increase to 16.54, and 12.66 GPa when the calcium silicate fraction reaches 70 wt% for C2S70, and C3S70. The indentation hardness shows values between 0.20 and 0.25 GPa for a lower content of CS (C_2S40, and C_3S40). These values increase above 0.60 GPa with 70 wt% of CS. For the C_2S series, the indentation modulus increases by 127%, and the indentation hardness increases by 186%. A similar but more modest increase is observed for the C_3S series: the indentation modulus increases by 14%, and the indentation hardness increases by 168%. A significant stiffening and strengthening of the inorganic polymer matrices is observed when considering Ca/Si and metakaolin geopolymer as strengthening additives. These results agree with those obtained for the three-point flexural strength tests (Fig. 8).

3.4.3. Fracture toughness

Fig. 10 displays the measured values of fracture toughness. A toughening effect is observed as the fraction of calcium silicate increases. When the C–S–H fraction is 40 wt%, the fracture toughness of the inorganic polymer cements is 0.25, 0.29, and 0.27 MPa m$^{1/2}$ for the
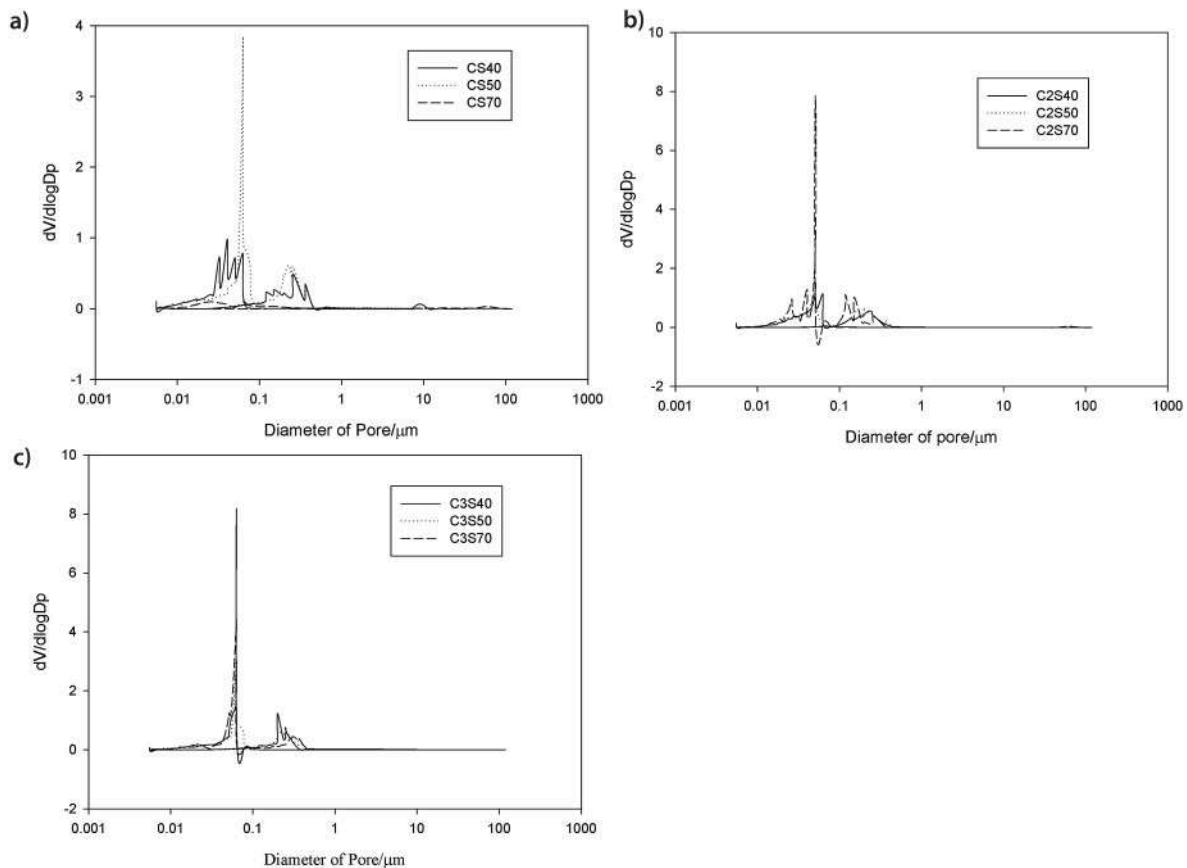
Fig. 5. Pore size distribution of inorganic polymer cement: a) CS series, b) C_2S series, and c) C_3S series.

CS, C_2S, and C_3S series. These values increase to 0.40, 0.48, and 0.375 when 70 wt% of C–S–H is used (Fig. 10). A significant increase in fracture toughness is observed with an increase in C–S–H. In particular, when the C–S–H fraction is increased from 40 to 70 wt%, the fracture toughness increases by 60% for the CS series, 66% for the C_2S series, and 38% for the C_3S series. Similarly, when the amount of silica is decreased from CS to C_3S, the fracture toughness decreases.

Fig. 11 displays the fracture micromechanisms and fracture scaling of inorganic polymer composites. Fig. 11a displays the residual groove after scratch testing conducted on an inorganic polymer composite, showing the presence of curved microcracks along with debris formation on the sides of the groove. Fig. 11 b–e display the observed toughening micromechanisms: microcracking, microcrack particle bridging, microcrack ligament bridging, and debris formation.

3.5. Microscopic phase analysis

BESEM shows the presence of two phases characterized by two length scales (Fig. 7). Here, statistical nanoindentation is employed to further explore the phase distribution of the synthesized inorganic polymer cement. The chemomechanical phases are identified based on their mechanical signatures. For instance, the indentation modulus of metakaolin geopolymer (MK GP) lies within 5–11 GPa, depending on the Si/Al ratio. Duxson et al. (2005a,b) studied the mechanical properties of sodium-based geopolymer with an Si/Al ratio of 1.15–2.15 and they reported an optimal elastic modulus value of 5.5 GPa for Si/Al = 1.90. Duxson et al. (2007) studied the influence of alkali activator on the elastic modulus and concluded that potassium-based geopolymer exhibits a higher elastic modulus compared to sodium-based geopolymer. Akono (2020) conducted indentation tests on potassium-based metakaolin geopolymer with Si/Al = 2 and reported an indentation modulus of 8.5 GPa. Akono et al. (2019) showed that the indentation modulus of

potassium-based metakaolin geopolymer decreases as the microporosity increase with an asymptotic value of 12.5 GPa for the indentation modulus for a zero microporosity). Moreover, using nanoindentation combined with statistical deconvolution methods, Němeček et al. (2011) showed that the Young's modulus of the N-A-S-H gel is 17–18 GPa regardless of the curing procedure and of the source of aluminosilicates.

Figs. 12 and 13 display the results of the statistical deconvolution analysis for the nanoindentation tests conducted on specimens C_2S40, C_2S70, C_3S40, and C_3S70. The probability distribution function (PDF) of the indentation modulus, M, along with the individual experimental data, is shown in the (M,H) plan. For all inorganic polymer composites, two phases are observed—MK GP and N–C-A-S-H—which agrees with the BESEM observations of two phases with distinct morphology and length scales.

Table 2 displays the indentation modulus and hardness values for the individual microphases of inorganic polymer composites. C_2S40 exhibits 2 MK GP phases of indentation moduli 5.33 and 9.99 GPa and two N–C-A-S-H phases of indentation moduli 14.78 and 27.75 GPa C_2S70 comprises one MK GP phase of indentation modulus 8.52 GPa and three N–C-A-S-H phases of indentation moduli 22.33, 30.36, and 37.61 GPa C_3S40 comprises one MK GP phase of indentation modulus 8.52 GPa and three N–C-A-S-H phases of indentation moduli 14.67, 20.23, and 26.40 GPa. Finally, C_3S70 exhibits one MK GP phase of indentation modulus 6.82 GPa and three N–C-A-S-H phases of indentation moduli 16.02, 23.50, and 37.41 GPa.

Fig. 14 displays the fraction of MK GP vs. N–C-A-S-H phases in inorganic polymer composites. The fraction of MK GP decreases from 90% in C_2S40 down to 78% in C_2S70, while that of N–C-A-S-H increases from 10% in C_2S40 to 22% in C_2S70. Similarly, the fraction of MK GP decreases from 75% in C_3S40 to 69% in C_3S70, while that of N–C-A-S-H increases from 25% in C_3S40 to 31% in C_3S70. The addition of CS content induces the conversion of MK GP into N–C-A-S-H phase. As a
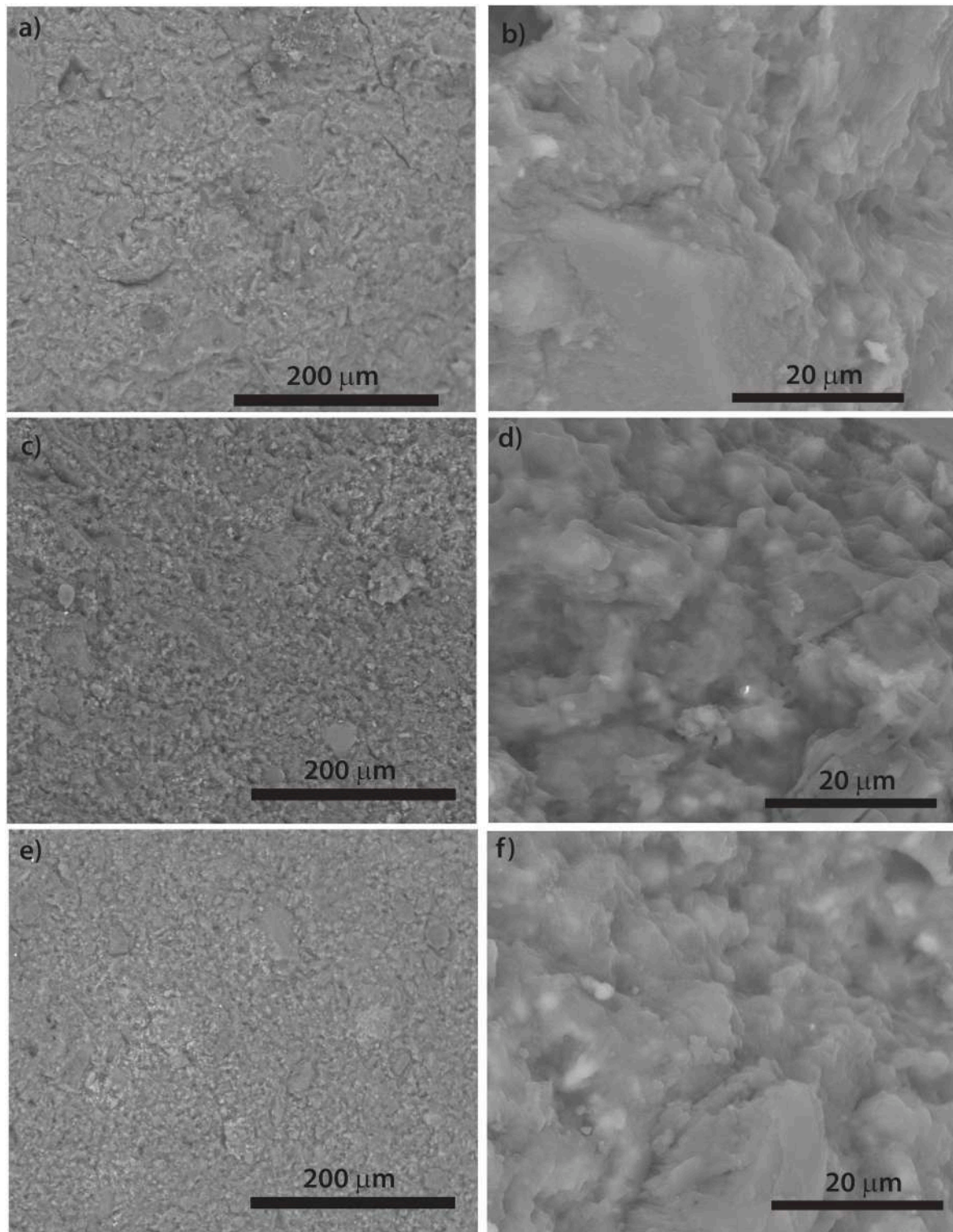
Fig. 6. Morphology of inorganic polymer cement: CS70 (a and b), C_2S70 (c and d), C_3S70 (e and f).

result of this conversion, higher mechanical properties are observed in terms of stiffness, strength, and fracture toughness.

4. Discussion

4.1. Integrating geopolymerization and calcium silicate hydration

Alkali-activated binders are fundamentally based on the principle of dissolution efficiency and polymerization/polycondensation of amorphous alumino-silicate precursors. The colloids formed after dissolution are oligomers of silicate and alumina having the intrinsic characteristics to self-polymerize/polycondense to form a binder. The mix of C–S–H and N-A-S-H in an alkaline solution results in a high rate of dissolution of silica and alumina with the formation of highly reactive oligomeric species, including $Al(OH)_4^-$ and $SiO_n(OH)_n^-$ monomers, which will polymerize and integrate Si–Ca chains into their interfaces. The
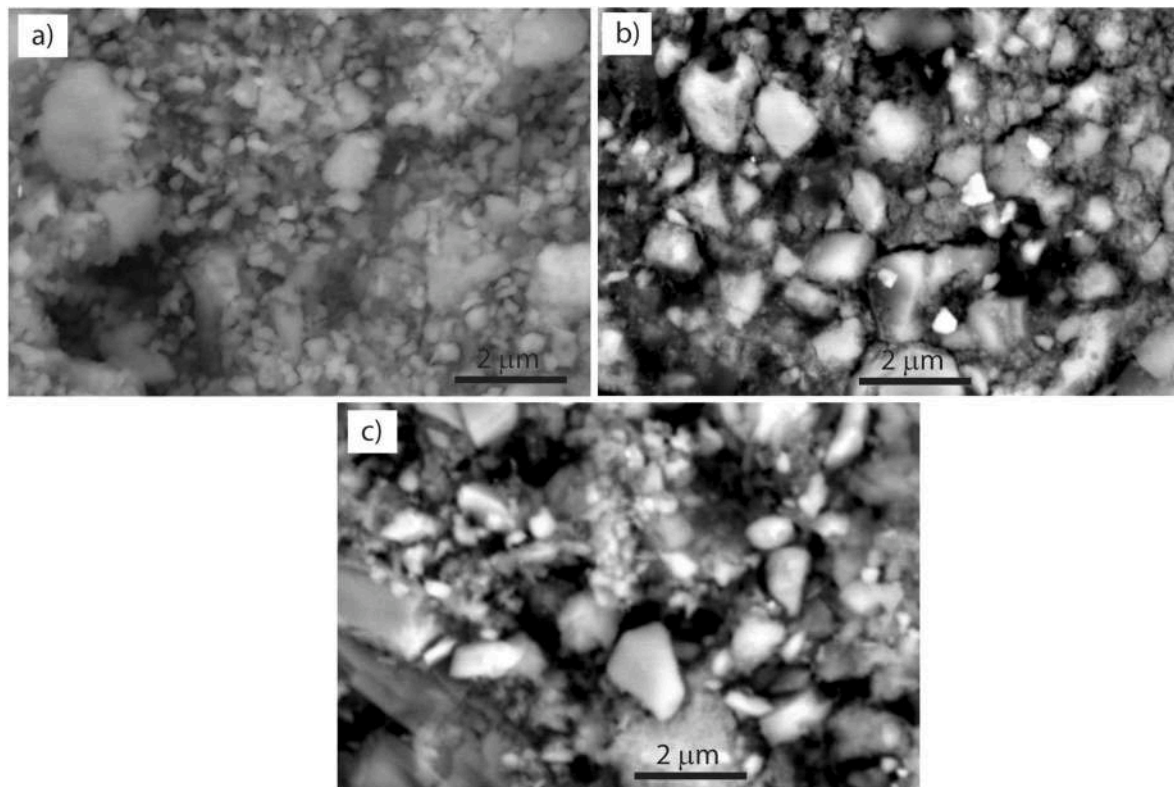
Fig. 7. Granular nature of inorganic polymer cement: a) CS70, b) C_2S70, and c) C_3S70.
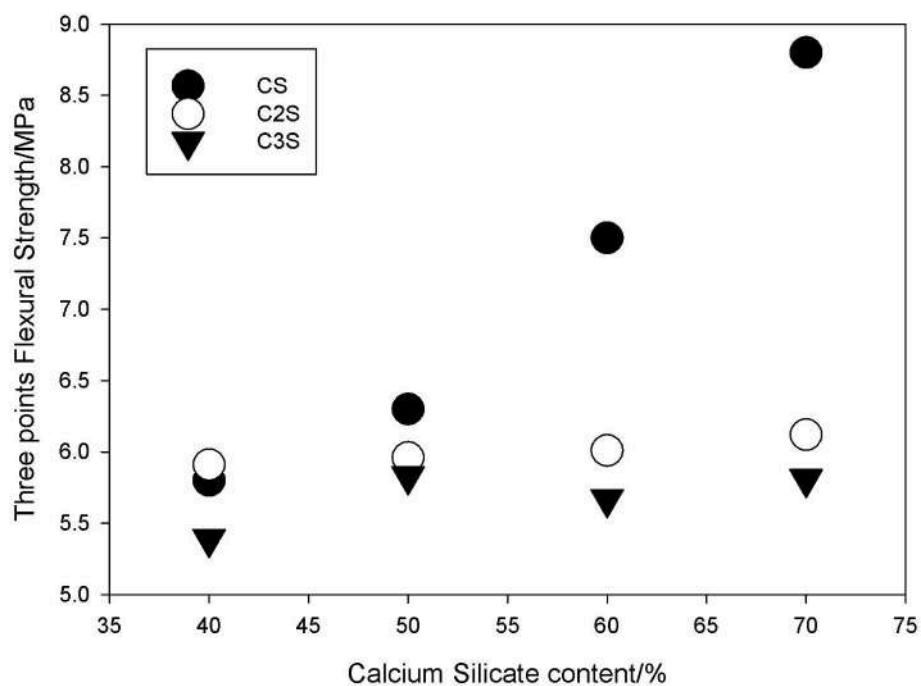

Fig. 8. Three-point flexural strength of inorganic polymer cement as a function of calcium silicate content.

observed homogeneous microstructure suggests the simultaneous dissolution of the solid precursors (metakaolin and calcium silicate) with a high extent of polymerization and polycondensation, which are responsible for the even distribution of (N)–C-A-S-H phases. These high degrees of dissolution and reactivity allow the binder to act more efficiently without or with a very low fraction of unreacted phases. These new metakaolin-based geopolymer binders can be compared to fly ash or slag-based C-A-S-H binders in terms of their efficiency to embed aggregates (Lloyd et al., 2009). The microstructure of the final gel appears different from that of the abovementioned gel because of the particular ability of C–S–H and N-A-S-H colloids to embed aggregates, interlocked with finer particles filling the interstitial porosity. Na+ and Al^{3+} can act in the transitional structure, putting together two molecules of C–S–H and N-A-S-H with the final microstructure having less porosity, suitable
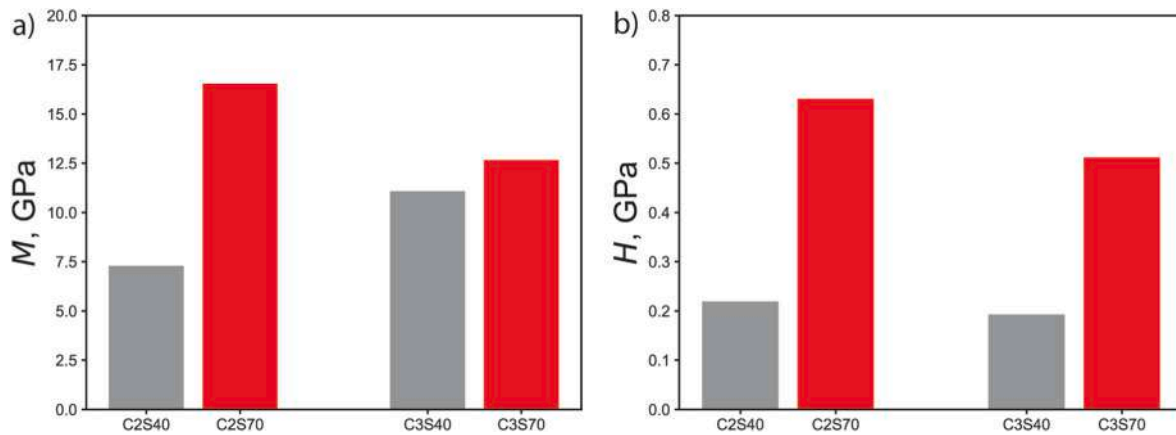
Fig. 9. Influence of calcium silicate content on elasto-plastic characteristics of inorganic geopolymers: a) average indentation modulus M. b) Average indentation hardness H for the tested specimens. N = 256 indentation tests were performed for specimens C_2S40 and C_3S40, and N = 441 indentation tests were performed for the remaining specimens.
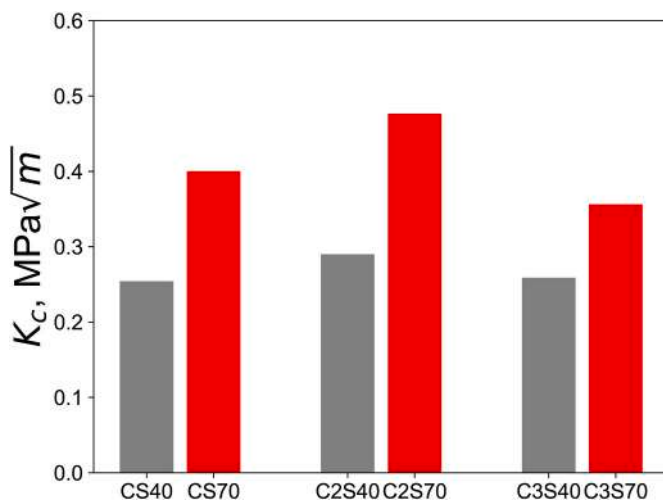

Fig. 10. Fracture toughness K_c of inorganic polymer composite specimens. N = 8 tests were conducted for each specimen.

densification, and compactness. The homogeneous distribution of the gel results from prolonged reactions of the dissolution of aluminosilicates to CS hydration.

4.2. Role of silica in densifying, stiffening, strengthening, and toughening

The amount of silica has a significant influence on the chemical structure and microstructure of the resulting inorganic polymer cement. The gel produced in this study exhibits homogeneous distribution, particularly when the dissolved silica is present in a significant amount. The globular units developed are very fine in size with high connectivity, making them ready to homogeneously distribute the mechanical stresses when under load. The C_2S40 matrix presents a more porous microstructure with a relatively high cumulative pore volume (0.291 mL g^{-1} compared to CS40 (0.23 mL g^{-1})). The interstitial spaces within the gel constitute an important fraction of the binder' porosity (Fig. 4b). Even though the gel here appears less dense due to the interlayer nature of C–S–H phases that constitute the basic gel structure before reinforcement, the insertion of Al-based geopolymer gel from MK is efficient in controlling porosity (Fig. 5). The decrease in silica content in the calcium silicate reduces the densification of the gel and increases the porosity, particularly the nanoporosity. The greater the silica concentration in the gel, the greater is the globular unit presenting a similar size

and homogeneous feature throughout the matrix, whether at the surface or in bulk. In N(C)-A-S-H gel systems, the covalent bonds controlled with the silica concentration are the bonds responsible for optimum polycondensation. This explains the fundamental difference in the three classes of inorganic polymer cement. In fact, the increase in the silica content significantly increases the potential of formation of long polymeric chains, while in the case of low silica (C_2S and C_3S) content, more monomeric oligomers are formed. In high concentrations of silica, aluminum can replace silicon in many of the oligomeric anions that occur (Swaddle et al., 1994).

These results suggest that silica only partially participates in the formation of C-A-S-H and amorphous geopolymer. The excess silica acts as an additional binder, as it takes the form of colloids with the potential to bind the matrix. This part contributes to the matrix densification, particularly when the pore solution is alkaline, as the volume of pores and their interconnectivity are modified with the action of colloidal silica. The potential formation of sodium silicate gel is hypothesized. This sodium silicate plays a significant role in closing the porosity, which explains the increase in density in the resulting inorganic polymer cements. This trend is evident when the C–S–H fraction exceeds 50 wt%.

4.3. Broader engineering relevance

This study shows that marble waste can be successfully valorized by concurrent mixing with rice husk ash and activation with metakaolin. Our study agrees with prior work (Komnitsas et al., 2021) as we observe the formation of a hybrid N–C-A-S-H phases. Whereas other studies reported an increase in porosity (Komnitsas et al., 2021) for marble-derived alkali activated materials, our approach leads to a compact microstructure with a lower porosity.

When calcium silicates are designed from marble waste powders, high-grade cementitious materials are produced with fine particle size and high values of Brunauer–Emmett–Teller surface area (Kamseu et al., 2021b). In this study, the microstructure achieved when calcium silicate is activated simultaneously with metakaolin in a geopolymerization context (alkaline media with colloid silica available) is compact with high strength and low porosity with a significant stiffening, strengthening, and toughening action of the metakaolin. In particular, the mix of C–S–H and geopolymer, N–C-A-S-H, appears as a binder that can achieve more than 90% reactivity of its particles. Inorganic polymers derived from marble wastes lead to binders with suitable binding strength, elastic properties, and fracture toughness, compared to ordinary Portland cement and geopolymer cement. This study has demonstrated the potential of valorizing marble wastes and rice husk ashes with low-temperature alkali activation, which is environmentally friendly and sustainable. The next step is to study the durability and long-term
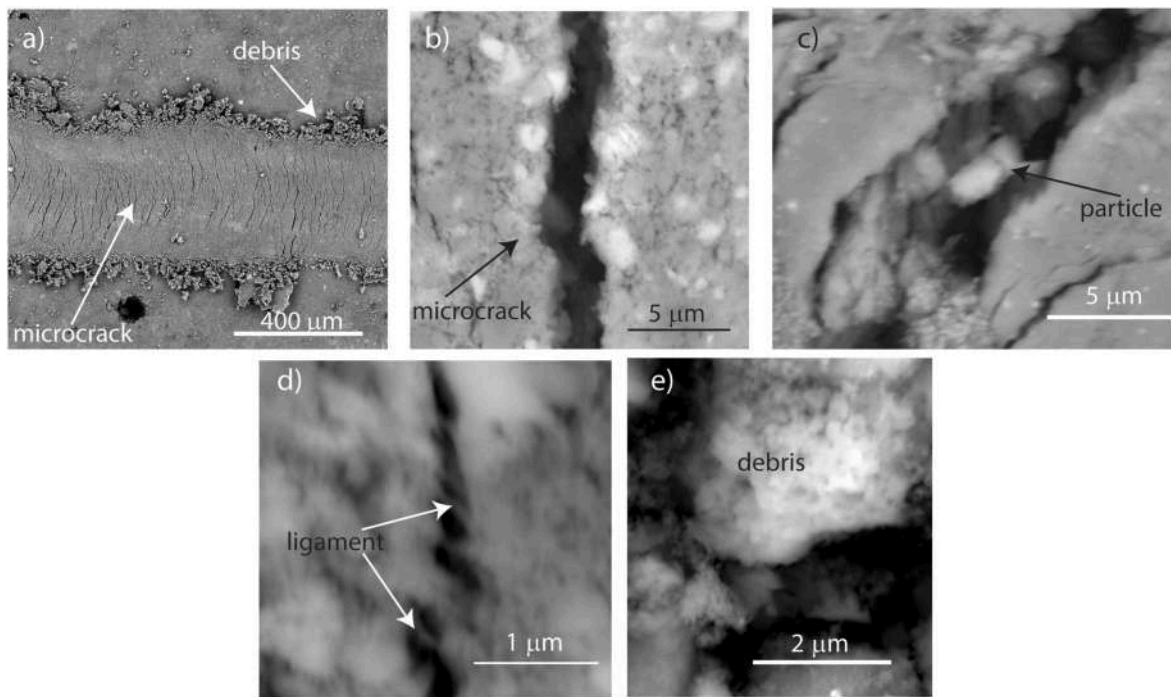
Fig. 11. Fracture micromechanisms and fracture scaling of inorganic polymer composite probes through scratch tests. a) Residual groove after scratch testing. b) Microcrack. c) Particles bridging a microcrack. d) Ligaments bridging a microcrack. e) Debris formed during scratching. f) Fracture scaling of the scratch test. F_T is the horizontal force, 2 pA is the scratch probe shape function area, d is the penetration depth, and K_c is the fracture toughness.
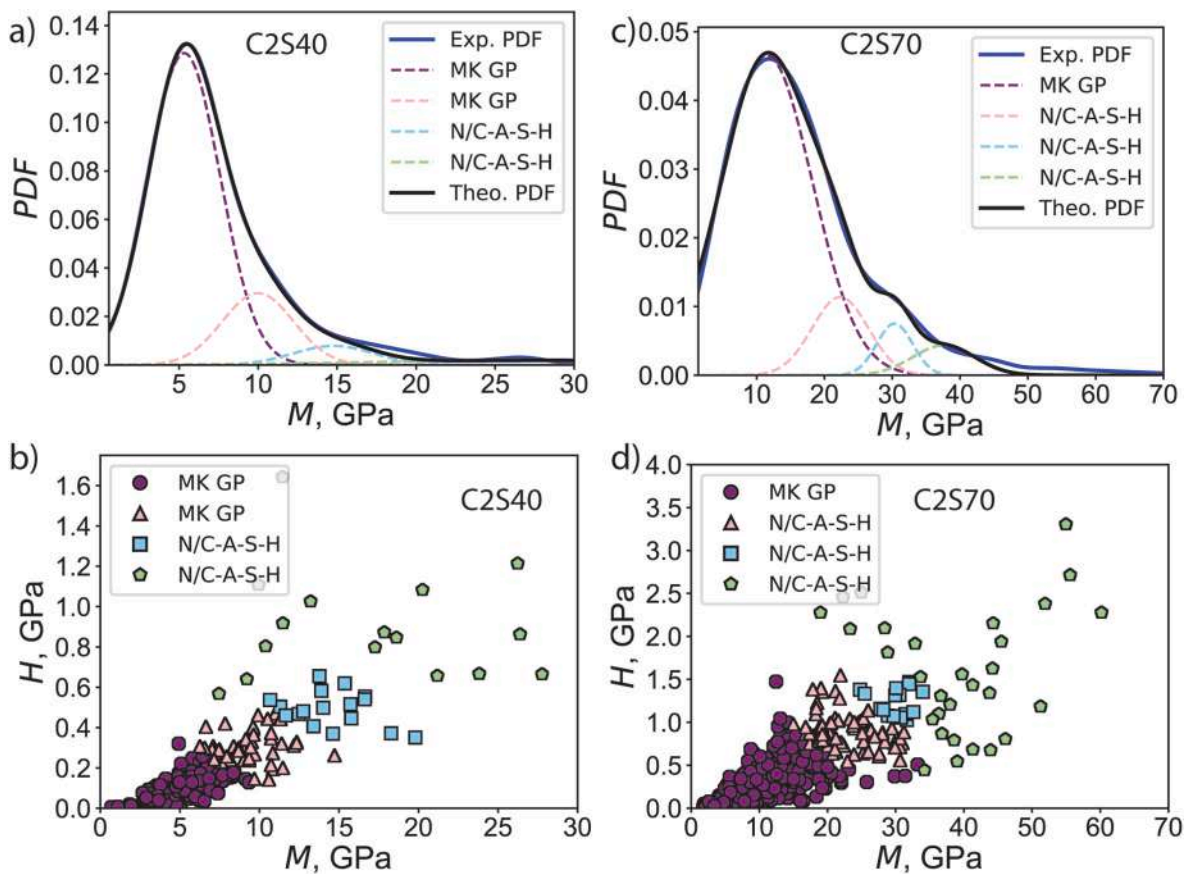
Fig. 12. Statistical deconvolution analysis of indentation data for inorganic polymer composites C_2S40 and C_2S70. PDF = probability distribution function. M is the indentation modulus and H is the indentation hardness. MK GP = amorphous metakaolin geopolymer. N/C-A-S-H = sodium/calcium aluminosilicate hydrates.
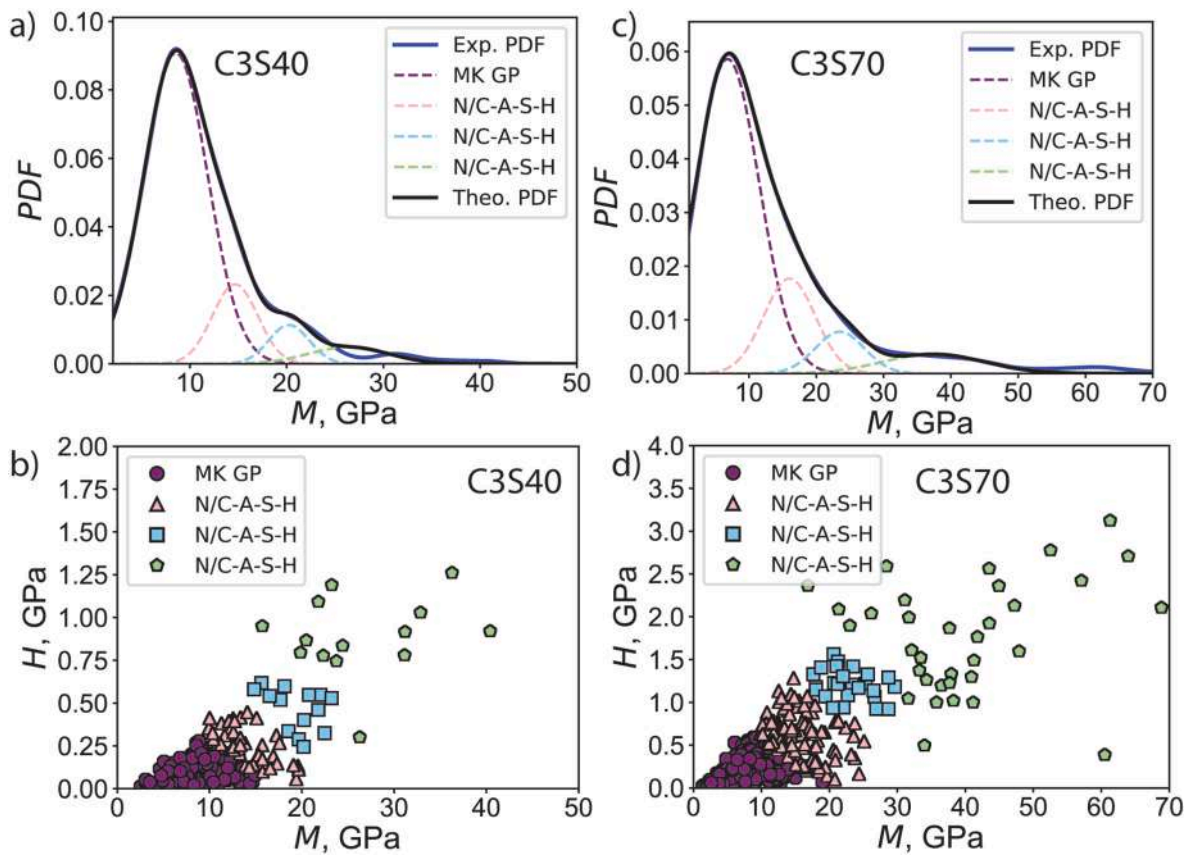
Fig. 13. Statistical deconvolution analysis of indentation data for inorganic polymer composites C$_3$S40 and C$_3$S70. PDF = probability distribution function. M is the indentation modulus, and H is the indentation hardness. MK GP = amorphous metakaolin geopolymer. N/C-A-S-H = sodium/calcium aluminosilicate hydrates.
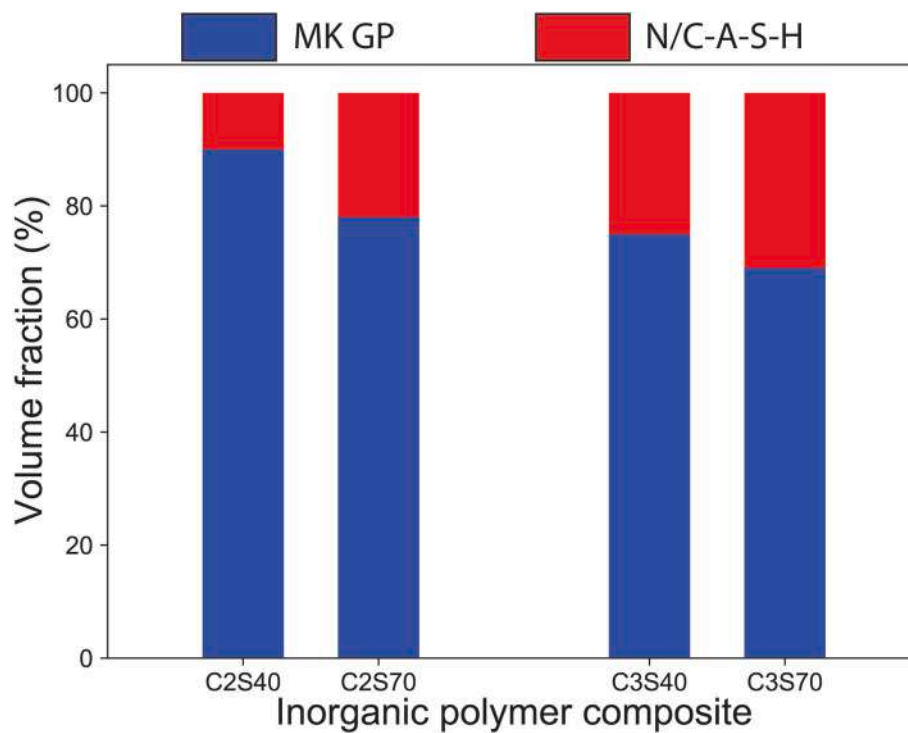

Fig. 14. Influence of calcium silicate content on the phase distribution of inorganic geopolymer composites. MK GP = amorphous metakaolin geopolymer. N/C-A-S-H = sodium/calcium aluminosilicate hydrates.

response of inorganic polymer cements derived from marble waste combined with rice husk ash.

5. Conclusions

From the results, the following conclusion can be drawn:

- When C–S–H and N-A-S-H pastes are mixed, the resulting inorganic polymer exhibits both an amorphous phase and crystalline phase, of chemical formula N–C-A-S-H. The fraction of the crystalline phase increases as the fraction of C–S–H increases and as the Ca content of the C–S–H increases.
- The decrease in the silica content from CS to C_2S and C_3S leads to a decrease in the wavelength of the peak of the principal FT-IR band, indicating a reduction of the amount of Q^3 and Q^4 silicon environment, which is characteristic of amorphous phases.
- The flexural strength varies from 5.5 to 8.7 MPa for the inorganic polymer cements. In general, the flexural strength increases when the silica content is low, from CS, C_2S, to C_3S. The flexural strength also increases when the fraction of calcium silicate hydrates increases.
- The fracture toughness of the inorganic polymer cements ranges from 0.25 to 0.48 MPa m$^{1/2}$. The highest values of fracture toughness are observed for the CS and C_2S systems with a 70 wt% fraction of calcium silicate hydrates.
- The bulk density of inorganic polymer cements ranges from 1.4 to 1.7 g/cm^3. The cumulative pore volume ranges from 0.23 to 0.29 mL/g. The dominance of calcium silicate in the mix results in a reduction in the pore size in all formulations. In addition, the fraction of gel pores of less than 20 nm in diameter significantly decreases when the fraction of calcium silicate hydrates increases.
- Backscattering environmental scanning electron microscopy reveals a homogeneous microstructure with high compactness for the inorganic polymer cements. A multiphase structure is observed with two phases, metakaolin geopolymer and N–C-A-S-H, which are characterized by two length scales: approximately 30 nm and 150–250 nm.
- Inorganic polymer cements derived from marble wastes exhibit characteristics similar to those of ordinary Portland cement and metakaolin-based geopolymers in terms of reactivity and binder capacity, with a low amount of unreacted phases during the activation.

In brief, given their homogeneous and compact microstructure, elastic properties, flexural strength, and fracture toughness, inorganic polymer cements derived from marble wastes appear to be promising candidates for innovative low-temperature binders with low carbon footprints to meet the sustainability requirements while satisfying the local material concept. In future studies, we will investigate the durability and long-term response of inorganic polymer cements derived from marble waste combined with rice husk ash.

Conflict of interest

The authors of this paper declare no conflict of interest.

Acknowledgments

References

Akono, A.T., 2020. Fracture behavior of metakaolin-based geopolymer reinforced with carbon nanofibers. Int. J. Ceram. Eng. Sci. 2, 234–242.

Akono, A.-T., Koric, S., Kriven, W.M., 2019. Influence of pore structure on the strength behavior of particle-and fiber-reinforced metakaolin-based geopolymer composites. Cement Concr. Compos. 104, 103361.

Akono, A.-T., Ulm, F.-J., 2014. An improved technique for characterizing the fracture toughness *via* scratch test experiments. Wear 313, 117–124.

Akono, A.-T., Randall, N.X., Ulm, F.J., 2012. Experimental determination of the fracture toughness *via* micro scratch tests: application to polymers, ceramics and metals. J. Mater. Res. 27, 485–493.

Akono, A.-T., Ulm, F.-J., 2012. Fracture scaling relations of axisymmetric shape. J. Mech. Phys. Solid. 60, 379–390.

Akono, A.-T., Reis, P.M., Ulm, F.-J., 2011. Scratching as a fracture process: from butter to steel. Phys. Rev. Lett. 106, 204302-104305.

Allen, A.J., Thomas, J.J., Jennings, H.M., 2007. Composition and density of nanoscale calcium-silicate in cement. Nat. Mater. 6, 311–316.

Alyousef, R., Benjeddou, O., Soussi, C., Khadimallah, M.A., Mustafa Mohamed, A., 2019. Effects of incorporation of marble powder obtained by recycling waste sludge and limestone powder on rheology, compressive strength, and durability of self-compacting concrete. Adv. Mater. Sci. Eng. https://doi.org/10.1155/2019/4609353.

Ashraf, W., Olek, J., 2016. Carbonation behavior of hydraulic and non-hydraulic calcium silicates: potential of utilizing low-lime calcium silicates in cement-based materials. J. Mater. Sci. 51, 6173–6191.

Avet, F., Boehm-Courjault, K., Scrivener, K., 2019. Investigation of C-A-S-H composition, morphology and density in limestone calcined clay cement (LC^3). Cement Concr. Res. 115, 70–79.

Benjeddou, O., Alyousef, R., Mohammadhosseini, H., Soussi, C., Khadimallah, M.A., Alabduljabbar, H., Tahir, M.M., 2020. Utilisation of waste marble powder as low-cost cementing materials in the production of mortar. J. Build. Eng. 32, 101642. https://doi.org/10.1016/j.jobe.2020.101642.

Carter, G., Smith, D.K., 1958. Properties of cementing compositions at elevated temperatures and pressure. Trans. AIME 213, 20—27.

Chindaprasirt, P., Sriopas, B., Phosri, P., Yoddumrong, P., Anantakarn, K., Kroehong, W., 2022. Hybrid high calcium fly ash alkali-activated repair material for concrete exposed to sulfate environment. J. Build. Eng. 45, 103590. https://doi.org/10.1016/j.jobe.2021.103590.

Dharmawardhanaa, C.C., Misrab, A., Ching, W.-Y., 2018. Theoretical investigation of C-(A)-S-H(I) cement hydrates. Construct. Build. Mater. 184, 536–548.

Duxson, P., Mallicoat, S.W., Lukey, G.C., Kriven, W.M., van Deventer, J.S.J., 2007. The effect of alkali and Si/Al ratio on the development of mechanical properties of metakaolin-based geopolymers. Colloid. Surf. A Physicochem. Eng. Aspects 292, 8–20.

Duxson, P., Provis, J.L., Lukey, G.C., Mallicoat, S.W., Kriven, W.M., van Deventer, J.S.J., 2005a. Understanding the relationship between geopolymer composition, microstructure and mechanical properties. Colloid. Surf. A Physicochem. Eng. Aspects 269, 47–58.

Duxson, P., Provis, J.L., Lukey, G.C., Separovic, F., van Deventer, J.S.J., 2005b. Si NMR study of structural ordering in aluminosilicate geopolymer gels. Langmuir 21, 3028–3036.

Fernandez-Jimenez, A., Palomo, A., Sobrados, I., Sanz, J., 2006. The role played by the reactive alumina content in the alkaline activation of fly ashes. Microporous Mesoporous Mater. 91, 111–119. https://doi.org/10.1016/j.micromeso.2005.11.015.

Habert, G., de Lacaillerie, J.B.D., Roussel, N., 2011. An environmental evaluation of geopolymer based concrete production: reviewing current research trends. J. Clean. Prod. 19, 1229–1238.

Kamseu, E., Alzari, V., Nuvoli, D., Sanna, D., Lancellotti, I., Mariani, A., Leonelli, C., 2021a. Dependence of the geopolymerization process and end-products to the nature of solid precursors: challenge of the sustainability. J. Clean. Prod. 278, 123587.

Kamseu, E., Alzari, V., Rosa, R., Nuvoli, D., Sanna, D., Mariani, A., Leonelli, C., 2021b. Marble wastes recycling: design and synthesis of low-temperature calcium silicate hydrate under various CaO:SiO$_2$ Ratio and alkalinity. Materialia 20, 10224–10233.

Kamseu, E., Bignozzi, M.C., Melo, U.C., Leonelli, C., Sglavo, V.M., 2013. Design of inorganic polymer cements: effects of matrix strengthening on microstructure. Construct. Build. Mater. 38, 1135–1145.

Kechagia, P., Koutroumpi, D., Bartzas, G., Peppas, A., Samouhos, M., Deligiannis, S., Tsakiridis, P.E., 2021. Waste marble dust and recycled glass valorization in the production of ternary blended cements. Sci. Total Environ. 761, 143224. https://doi.org/10.1016/j.scitotenv.2020.143224.

Komnitsas, K., Soultana, A., Bartzas, G., 2021. Marble waste valorization through alkali activation. Minerals 11, 46. https://doi.org/10.3390/min11010046.

Kriven, W.M., Bell, J.L., Gordon, M., 2006. Microstructure and nanoporosity of as-set geopolymers, mechanical properties and performance of engineering ceramics II. Ceram. Eng. Sci. Proc. 27, 491–503.

Kuzielová, E., Žemlička, M., Másilko, J., Palou, M.T., 2017. Pore structure development of blended G-oil well cement submitted to hydrothermal curing conditions. Geothermics 68, 86—93.

Li, N., Zhang, Z., Shi, C., Zhang, J., 2018. Some progresses in the challenges for geopolymer. In: IOP Conf. Ser.: Mater. Sci. Eng., 431, 022003.

Liu, Y., Shi, C., Zhang, Z., Li, N., 2019. An overview on the reuse of waste glasses in alkali-activated materials. Resour. Conserv. Recycl. 144, 297–309.

Lloyd, R.R., Provis, J.L., van Deventer, J.S., 2009. Microscopy and microanalysis of inorganic polymer cements. 2: the gel binder. J. Mater. Sci. 44, 620–631.

Matsuyana, H., Young, J., 2008. Effects of pH on precipitation of quasi-crystalline calcium silicate hydrate in aqueous solution. Adv. Cement Res. 12, 29–33.

Mehta, D., Paliwal, D., Singh Sankhla, V., Tege, S., 2020. Study of marble waste and its utilization. Int. Res. J. Eng. Technol. 7, 1–5. https://www.irjet.net/archives/V7/i7/IRJET-V7I701.pdf.

Myers, R.J., Bernal, S.A., San Nicolas, R., Provis, J.L., 2013. Generalized structural description of calcium-sodium aluminosilicate hydrate gels: the crosslinked substituted tobermorite model. Langmuir 29, 5294–5306.

Němeček, J., Šmilauer, V., Kopecký, L., 2011. Nanoindentation characteristics of alkali-activated aluminosilicate materials. Cement Concr. Compos. 33, 163–170.

Oliver, W.C., Pharr, G.M., 1992. An improved technique for determining hardness and elastic modulus using load and displacement sensing indentation experiments. J. Mater. Res. 7, 1564–1583.

Provis, J.L., 2018. Alkali-activated materials, cem. Concr. Res. 114, 40–48.

Provis, J.L., Lukey, G.C., van Deventer, J.S.J., 2005. Do geopolymers actually contain nanocrystalline zeolites: a reexamination of existing results. Chem. Mater. 17, 3075.

Ribeiro, R.A.S., Ribeiro, M.S., Kriven, W.M., 2017. A review of particle-and fiber-reinforced metakaolin-based geopolymer composites. J. Ceram. Sci. Technol. 8, 307–322.

Richardson, L.G., 2008. The calcium silicate hydrates. Cement Concr. Res. 38, 137–158.

Rodrigues, F.A., 2003. Low-temperature synthesis of cements from rice hull ash, Cem. Concr. Res. 33, 1525–1529.

Rovnaník, P., 2010. Effect of curing temperature on the development of hard structure of metakaolin-based geopolymer. Construct. Build. Mater. 24, 1176–1183.

Sharma, N., Kumar, R., 2015. Use of waste marble powder as partial replacement in cement sand mix. Int. J. Eng. Res. Technol. 4, 501—504.

Shi, C., Fernández-Jiménez, A., Palomo, A., 2011. New cements for the 21st century: the pursuit of an alternative to Portland cement. Cement Concr. Res. 41, 750–763.

Swaddle, T.W., Salerno, J., Tregloan, P.A., 1994. Aqueous aluminates, silicates and aluminosilicates. Chem. Soc. Rev. 23, 319–325.